

PCCP

Accepted Manuscript



This is an *Accepted Manuscript*, which has been through the Royal Society of Chemistry peer review process and has been accepted for publication.

Accepted Manuscripts are published online shortly after acceptance, before technical editing, formatting and proof reading. Using this free service, authors can make their results available to the community, in citable form, before we publish the edited article. We will replace this *Accepted Manuscript* with the edited and formatted *Advance Article* as soon as it is available.

You can find more information about *Accepted Manuscripts* in the [Information for Authors](#).

Please note that technical editing may introduce minor changes to the text and/or graphics, which may alter content. The journal's standard [Terms & Conditions](#) and the [Ethical guidelines](#) still apply. In no event shall the Royal Society of Chemistry be held responsible for any errors or omissions in this *Accepted Manuscript* or any consequences arising from the use of any information it contains.



Physical Chemistry Chemical Physics

PAPER

Thickness-Induced Structural Phase Transformation of Layered Gallium Telluride

Q. Zhao,^a T. Wang,^{*a} Y. Miao,^b F. Ma,^{*b} Y. Xie,^c X. Ma,^{*c} Y. Gu,^a J. Li,^a J. He,^a B. Chen,^a S. Xi,^a L. Xu,^a H. Zhen,^a Z. Yin,^a J. Li,^a J. Ren,^a and W. Jie^a

Received 00th January 20xx,
Accepted 00th January 20xx

DOI: 10.1039/x0xx00000x

www.rsc.org/

Thickness-dependent electronic states and physical properties of two-dimensional materials suggest great potential applications in electronic and optoelectronic devices. However, the enhanced surface effect in the ultra-thin materials might significantly influence the structural stability as well as the device reliability. Here, we report a spontaneous phase transformation of Gallium Telluride (GaTe) when the bulk was exfoliated to few layers. Transmission electron microscopy (TEM) results indicate a structure variation from monoclinic to hexagonal one. Raman spectra suggest a critical thickness for the structural transformation. First-principle calculations and thermodynamic analysis shows that, the surface energy and the interlayer interaction compete to dominate structural stability in the thinning process. A two-stage transformation process from monoclinic (m) to tetragonal (T) and then from tetragonal to hexagonal (h) is proposed to understand the phase transformation. The results demonstrate the crucial role of interlayer interaction on the structural stability, which supplies a phase-engineering strategy for device applications.

Introduction

Two-dimensional (2D) materials, bonded through van der Waals force, commonly exhibit thickness-dependent electronic states and physical properties.¹⁻⁹ For example, the band gap changes from indirect into direct resulting in strong light-matter interaction as bulk MoS₂ is exfoliated into monolayer ones,¹ topological phase transformation takes place in few-layer Bi₂Se₃,² the band gap of 2D black phosphorus decreases from 1.51 eV to 0.59 eV by 61% with thickness reduced from five layers to monolayer.³ As a result, the electronic and optical properties of 2D materials could be substantially tuned by reducing the thickness, which makes them promising candidates in next-generation electronic and optoelectronic devices. On the other hand, when the feature sizes of materials are reduced down to nanometer scale, the surface effect will become dominant on the structural stability, and even lead to

spontaneous phase transformation or reorientation.^{10, 11} For the laminated compounds, the surface effect and interlayer coupling might compete to promote phase transition in few-layer systems. Accordingly, unexpected structure and physical properties might be induced, on which more attentions should be paid in the applications.

Gallium Telluride (GaTe), a promising candidate in electronic and optoelectronic devices with high photoresponsivity of 10⁴ A/W for few-layer sheets,¹²⁻¹⁴ provides us a great insight on structure evolution with thickness because of its unique structure features. Different from other III-VIA layered compounds, such as, GaS,¹⁵ GaSe and InSe,^{16, 17} the atoms in bulk GaTe are arranged in monoclinic lattice instead of hexagonal one. Two kinds of Ga-Ga bonds are involved in GaTe: one third along the in-plane direction in the layers but two thirds perpendicular to the layers.¹⁸ Hence, the lattice structure of GaTe becomes more complicated. This might lead to unusual structural stability and consequently extraordinary properties in few-layer GaTe. In this work, a phase transformation from monoclinic structure to hexagonal one was observed in the few-layer flakes by TEM and Raman spectra. The thermodynamic analysis based on the density functional theory was conducted. A two-stage model was proposed to understand the thickness dependent phase transformation. The results demonstrate the crucial role of interlayer interaction on the structural stability of the layered compound and provide useful guidance for phase engineering of GaTe.

Experimental

^aState Key Laboratory of Solidification Processing, Northwestern Polytechnical University, Xi'an, 710072, P. R. China. E-mail: taowang@nwpu.edu.cn

^bState Key Laboratory for Mechanical Behavior of Materials, Xi'an Jiaotong University, Xi'an, 710049, P. R. China. E-mail: mafei@mail.xjtu.edu.cn

^cState Key Discipline Laboratory of Wide Band Gap Semiconductor Technology, School of Advanced Materials and Nanotechnology, Xidian University, Xi'an, 710071, P. R. China. E-mail: xhma@xidian.edu.cn

†Electronic Supplementary Information (ESI) available: XRD result of bulk GaTe. The SEM image of 2D GaTe fabricated by mechanical exfoliation. Low-temperature PL spectra of bulk GaTe. The locating pattern on the substrate. Derivation of the relationship between the total interaction potential E_{tot} and interlayer spacing Z . See DOI: 10.1039/x0xx00000x

Sample Fabrication

Single-crystal GaTe was grown by the Bridgman method. For bulk GaTe, the cleaved samples 10 mm×10 mm×1 mm in size were prepared by a razor blade. The sample surface are mirror-like and no further cleaning, polishing or etching treatment is required to improve the optical quality. Immediately after cleavage, the samples were put into the experiments to avoid oxidation on surface. Conductivity measurements showed that all the samples are *p*-type and the carrier density is in the order of 10^{15} - 10^{16} cm⁻³. 2D GaTe sheets were fabricated by liquid and mechanical exfoliation, respectively. In liquid exfoliation process, GaTe powder was mixed with ethanol solvent, and kept in ultrasonic vibrator for 24 hours. After centrifugal treatment, few-layer GaTe flakes were dispersed in the supernatant. For mechanical exfoliation, a three-step method, consisting of stripping, transferring and re-stripping, was employed to obtain large-area samples. Firstly, some GaTe flakes with the thickness of 6~8 μm were torn off from the bulks by a piece of scotch tape. Immediately, the flakes were exfoliated repeatedly until they were no longer shiny. The surface of GaTe flakes were fully contacted with the scotch tape and exfoliated along one direction. Then, GaTe flakes were transferred onto SiO₂ (300 nm) /Si substrates and stripping by scotch tape was done to reduce the thickness and prepare large-area 2D GaTe samples. All the samples were sequentially cleaned ultrasonically in acetone, methanol and isopropyl alcohol for 30 minutes, respectively, to remove the scotch tape residue. All the procedures were performed under an argon atmosphere to protect GaTe materials from being oxidized.

Structure and Morphology Characterization

The structure of bulk GaTe were characterized and analyzed by transmission electron microscopy (TEM, Tecnai F30 G2) with an energy-dispersion X-ray spectroscopy (EDS) attachment. For bulk GaTe, the samples were mechanically grinded down to a thickness of about 40 μm and ion beam thinning was done for TEM measurement. The liquid exfoliation in ethanol solvent for 24 h was adopted to prepare TEM samples of 2D GaTe. The surface morphology of the samples was observed with scanning electron microscopy (SEM, ZEISS-SUPRA-55). The thickness of the exfoliated GaTe nanosheets, in a range of 1-50 nm, was measured by atomic force microscopy (AFM, Veeco Dimension-Icon system).

Optical Characterization

In PL measurements, bulk GaTe was attached on a cold copper finger on a closed-cycle cryostat with grease to keep the temperature in the range of 10-50 K. A 20 mW argon ion laser with the wavelength of 488 nm was used to excite PL spectra and the incident laser spot was about 1 mm in diameter. The emitted signals were collected and analysed by a Triax 550 tri-grating monochromator with a photo-multiplier tube (PMT). The spatial resolution is better than 0.3 nm. Micro-Raman spectra were measured on a Renishaw Invia Laser—Raman Spectrometer at 300 K. Ar ion laser of 514.5 nm in wavelength

and 1 μm in spot diameter was used as excitation source. The incident light power was 5 mW. The back-scattering geometry was applied, in a way that both the incident light and the reflected Raman signals were perpendicular to the sample surface. The resolution in Raman spectra was 1 cm⁻¹, the accuracy of band positions was ± 0.1 cm⁻¹ and the frequency was above 100 cm⁻¹.

For 2D GaTe, micro-Raman measurements were conducted in the same condition mentioned above. The position of 2D GaTe flakes with different layer numbers was determined by the aid of a locating pattern in Fig. S1. The locating pattern on SiO₂ (300 nm) /Si substrate was a 40×40 square array fabricated by photolithography, and patterned Cr 5 μm × 5 μm in size was fabricated with a separation of 20 μm. Accordingly, the same flake could be found by optical microscopy, atom force microscopy (AFM) and micro-Raman instruments.

Calculation Details

First-principle calculations were carried out using the density functional theory (DFT) as implemented in MedeA-VASP. The monoclinic and hexagonal models are depicted in Fig. 2(a), 2(b) and 2(c), 2(d), respectively. The generalized gradient approximation with Perdew-Burke-Ernzerhof exchange-correlation potential (GGA-PBE) was used with a kinetic-energy cutoff of 600 eV. The *k*-point sampling was done according to the Monkhorst-Pack scheme. A *k*-point set of 11×11×11 was adopted for the calculation of bulk GaTe, while a *k*-point set of 11×11×1 was used for monolayer hexagonal GaTe. The structure was fully relaxed with an energy convergence of 1.0×10^{-5} eV and a force convergence of 0.01 eV/Å. Based on the optimized structures, the phonon dispersion curves of single-crystal GaTe were calculated and discussed in detail. 2×2 and 4×4 supercells were modeled to calculate the bulk energies of GaTe in monoclinic and hexagonal phases, respectively, in which 48 and 64 atoms were included. For the Brillouin-zone sampling, 9×9×9 *k* mesh according to Monkhorst-Pack scheme was used for the 2×2 supercells, but 7×7×1 for the 4×4 supercells. A cutoff energy of 600 eV was used along with a smearing factor of $\sigma = 0.1$ eV. The convergence was checked for all calculations.

As for the calculation of surface energy, the model of m-GaTe was built up firstly, then cleaved along (210) plane, and a vacuum slab with 10 Å in thickness was added to avoid the interaction between the top and bottom layers. 4×4 supercell composed of 64 atoms with a vacuum region 27 Å in thickness was built up to simulate a 2D hexagonal GaTe sheet. A *k*-point set of 11×11×1 was used for the monoclinic and hexagonal lattice. An energy cutoff of 600 eV was used along with a smearing factor of $\sigma = 0.1$ eV. The surface excess energy (E_{surf}) per atom on surface (N_{surf}) was determined as the difference between the total energy of a slab (E_{slab}) and that of the atoms in bulk environment with the energy per atom of E_{bulk}

$$E_{surf} = \frac{E_{slab} - NE_{bulk}}{N_{surf}} \quad (1)$$

Surface energy (γ) is indeed the surface excess energy per surface area and is expressed as

$$\gamma = \frac{E_{slab} - NE_{bulk}}{N_s A} = \frac{E_{slab} - NE_{bulk}}{A_{surf}}, \quad (2)$$

in which A is the surface area occupied by one atom on surface, and N_s is the number of atoms on surface in a unit cell.

Results and discussion

Transmission electron microscopy (TEM) was used to characterize the structure of both the bulk and 2D GaTe. Fig. 1(a) presents the selected area electron diffraction (SAED) pattern of bulk GaTe, which was ascribed to the monoclinic lattice. The lattice parameters in the reciprocal space are determined as $a^* = 0.0593 \text{ \AA}^{-1}$, $b^* = 0.0988 \text{ \AA}^{-1}$, $c^* = 0.2453 \text{ \AA}^{-1}$, $\alpha^* = \beta^* = 90^\circ$, $\gamma^* = 75.56^\circ$ and those in real space are $a = 17.404 \text{ \AA}$, $b = 10.456 \text{ \AA}$, $c = 4.077 \text{ \AA}$, $\alpha = \beta = 90^\circ$, $\gamma = 104.44^\circ$. Fig. 1(b) displays a high-resolution TEM (HR-TEM) image, and the high-quality single-crystal feature can be identified. A layered morphology with separation of 0.583 nm is observed and the cleavage plane can be indexed into (210), in good agreement with XRD result (Fig. S2). Low-temperature PL spectra of bulk GaTe (Fig. S3) were measured, the weak donor-acceptor pair (DAP) band and the sharp strong free exciton (FX) band are characteristic of low-defect-density and high-quality features.¹⁹ Few-layer GaTe was fabricated by mechanical and liquid exfoliation from the high-quality bulk GaTe. A representative SEM image of 2D GaTe nanoflakes on SiO₂ (300 nm) /Si substrate is shown in Fig. S4. The irregular

edge as well as the lamellar morphology is clearly observed. Fig. 1(c) shows a SAED pattern taken from 2D GaTe flake. Different from bulk GaTe, the spot pattern can be well indexed to hexagonal GaTe, in which structure parameters $a = 4.06 \text{ \AA}$, $b = 4.06 \text{ \AA}$, $c = 16.96 \text{ \AA}$, $\alpha = \beta = 90^\circ$, $\gamma = 120^\circ$ are determined. HR-TEM image of lattice structure is displayed in Fig. 1(d), a hexagonal arrangement can be clearly observed by the Fast Fourier Transformation (FFT) picture in the inset, corresponding to the region marked by red square. According to the TEM images, the models of monoclinic and hexagonal structures are built up. The top and side views of a two-layer primitive cell in monoclinic structure are shown in Fig. 2(a) and 2(b). Each Ga atom is surrounded by one Ga atom and three Te atoms, while each Te atom is bonded to three Ga atoms and participates in the weaker interlayer interaction with Te atom in the adjacent layer. The hexagonal structure is depicted in Fig. 2(c) and 2(d). Each layer consists of two AA-stacked hexagonal Ga sublayers sandwiched between two hexagonal Te sublayers. Obviously, a phase transformation from monoclinic structure to hexagonal one occurs when the bulk GaTe is exfoliated into 2D few-layer configuration.

Raman spectroscopy can provide rich information on crystal structure.²⁰ Fig. 3(a) presents the Raman spectrum of the as-prepared bulk GaTe from 100 cm^{-1} to 300 cm^{-1} at an excitation wavelength of 514.5 nm . Ten characteristic peaks are observed and match the reported data very well.^{21, 22} In order to reveal the origin of Raman peaks, the phonon dispersion curves of single-crystal GaTe are calculated by using first-principle method based on the established structure model (Fig. 2). Fig. 3(b) shows the calculated phonon dispersion curves in which 36 branches are involved: 3 of them are acoustic, 15 are infrared-active and 18 are Raman-active. No imaginary frequency is identified, which suggests that the bulk GaTe in monoclinic structure is dynamically stable. The eight Raman-active phonon frequencies corresponding to the experimental results are extracted from the phonon dispersion curve at reciprocal lattice point Γ . The calculated results and measured data are listed in

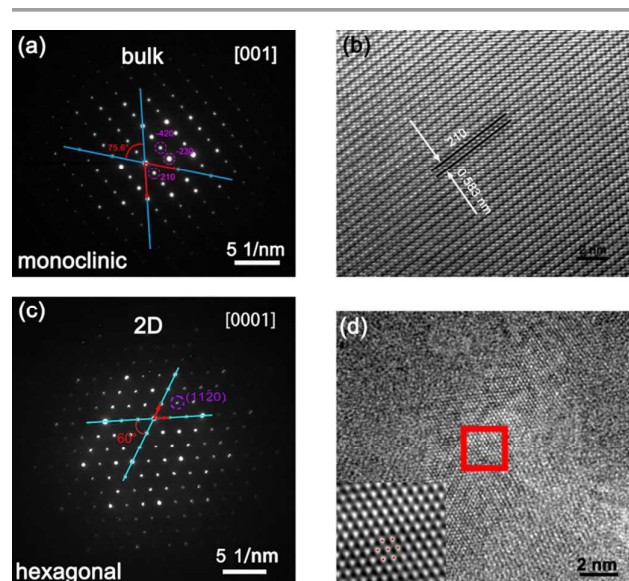


Fig. 1 HR-TEM images and selected area electron diffraction (SAED) patterns. (a) The SAED pattern of bulk GaTe along the [001] zone axial. (b) HR-TEM image of bulk GaTe cleaved from (210) plane with a separation of 0.583 nm . (c) The SAED pattern of 2D GaTe, indicating a hexagonal structure. (d) HR-TEM image of the 2D GaTe, and the inset displays the FFT image of the regions marked by a red square.

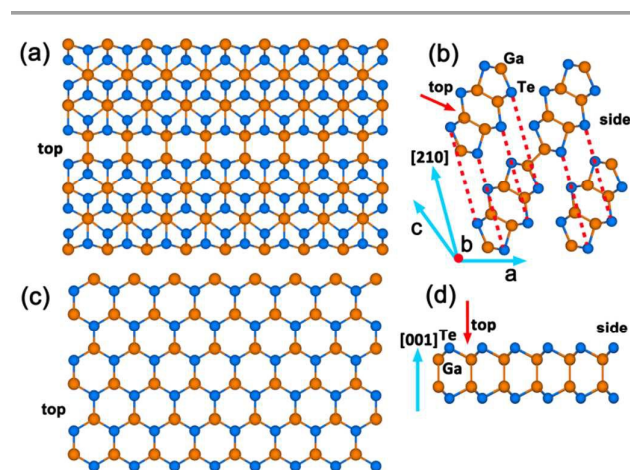


Fig. 2 The top and side views of monoclinic (a), (b) and hexagonal (c), (d) GaTe structure models.

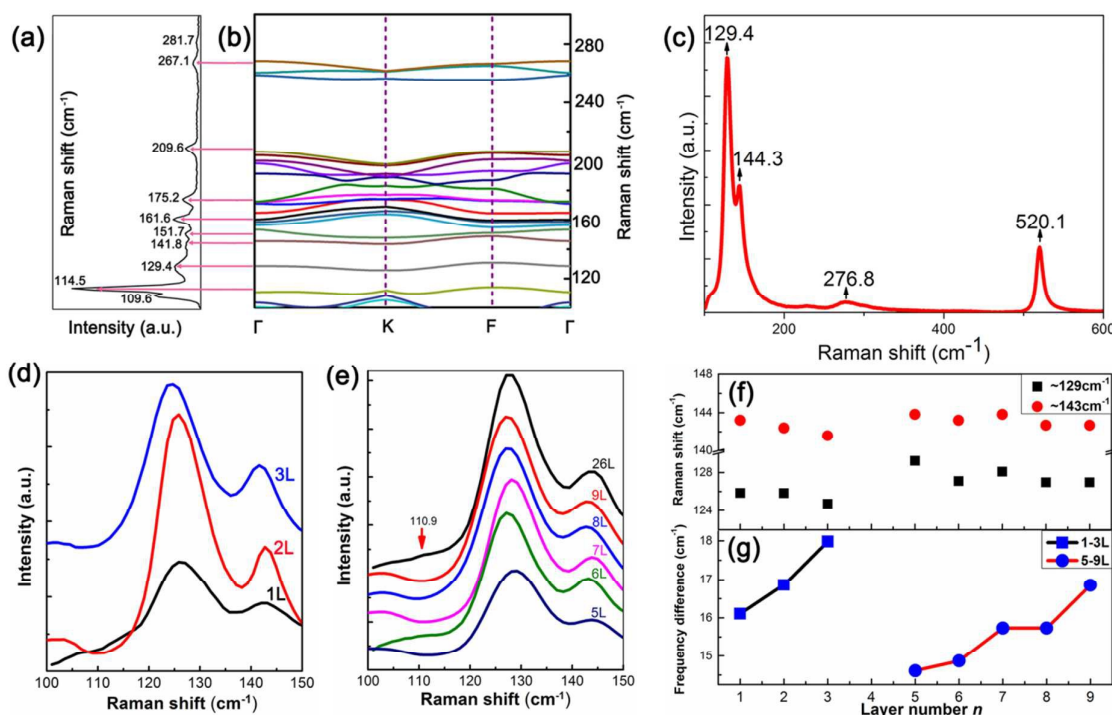


Fig. 3 Raman spectra of bulk and 2D GaTe. (a) Raman spectra of bulk GaTe at room temperature. (b) The calculated phonon dispersion curves. (c) Raman spectrum of 2D GaTe on SiO₂/Si substrate. (d) and (e) The Raman peaks of two A_g lattice vibration modes at 129 cm⁻¹ and 144 cm⁻¹ in GaTe with different thickness. (f) The position of the two A_g Raman-active modes at 129 cm⁻¹ and 144 cm⁻¹ as function of layer number *n*, respectively. (g) Frequency difference versus *n*.

Table S1 of support information. The small deviation between experimental and theoretical results might be due to the intrinsic surface stress because of the under-coordinated surface atoms and discrepancy of surface condition originated from defects in bulk GaTe.²³ Fig. 3(c) shows the Raman spectrum of 2D GaTe excited by 514.5 nm line in air ambient environment. The peaks at 129.4 cm⁻¹, 144.3 cm⁻¹ and 276.8 cm⁻¹ are ascribed to the lattice vibration in 2D GaTe and the peak at 520.1 cm⁻¹ is the characteristic of Si substrate. The Raman-active radiation is consistent with the results on few-layer GaTe grown by Molecular Beam Epitaxy (MBE).²⁴ Because of the multi-reflection of the incident laser at the interface and the interference of the Raman signal inside the layers, the Raman peak intensity of 2D GaTe is much stronger than that of bulk GaTe.²⁵ Similar enhancement in the Raman intensity has been reported for graphene and other layered compounds, such as Bi₂Se₃ and Bi₂Te₃.²⁵⁻²⁷ Fig. 3(d) and 3(e) present the Raman spectra evolution of GaTe sheets with various thicknesses at room temperature. The Raman shift of the two A_g lattice vibration modes, at 129 cm⁻¹ and 144 cm⁻¹ are shown in Fig. 3(f). Apparently, blue shift takes place with decreasing layer number owing to the reduced lattice constant induced and stiffened vibration mode by surface contraction. Similar blue shift of Raman-active mode E_{2g}¹ has been observed in few-layer MoS₂.⁴ The frequency difference was used to evaluate the sheet thickness for 2D materials.^{4, 6, 20} As shown in Fig. 3(g), the frequency difference decreases monotonously as the layer number is reduced from 9 to 5 and from 3 to 1. However, sharp change unexpectedly takes place in the four-layer GaTe sheet,

which might suggest a phase transformation from monoclinic to hexagonal lattice at the critical thickness of four layers.²⁸ This is consistent with the aforementioned results observed by HR-TEM. The two phases are denoted as m-GaTe and h-GaTe, respectively.

Thermodynamics analysis is conducted to determine the critical thickness for the phase transformation. As the bulk GaTe is exfoliated into few-layer ones, the interlayer separation is expanded as a result of weakened binding from adjacent atom layers.²⁹ The total interaction potential energy of Ga-Ga bonds and the adjacent layers E_{vdw} can be approximated by the following equation

$$E_{vdw} = -\frac{H}{6} \left[\frac{d}{2Z} + \frac{d}{2(Z+d)} + \ln \frac{d}{Z+d} \right] \quad (3)$$

in which d is the length of Ga-Ga bond, Z is the interlayer spacing, and H is a constant. The derivation can be found in support information. The relationship between the total interaction potential E_{vdw} and interlayer spacing Z is depicted in Fig. 4(a). It is clear that the interlayer spacing increases with the reducing layer number and the total interaction potential energy E_{vdw} increases correspondingly. The positive slope of variation curve dE_{vdw}/dZ indicates that additional energy is needed to increase the interlayer-interaction potential in this process. In general, the van der Waals force plays an important role in inhibition of phase transformation, which is of great significance for stabilization of the monoclinic phase.

Simultaneously, the surface-to-volume ratio becomes significantly large. The surface energy and surface stress become the dominant thermodynamic parameters governing the structural stability. Surface energy γ is usually defined as the reversible work needed to create a new surface per area in the system, and could be described by

$$\gamma = \frac{\delta W}{dA_s}, \quad (4)$$

in which δW is the reversible work and A_s is the new surface area. When a given n -layer GaTe sheet is thinned down to $(n-1)$ layer, the surface energy per area changes little, while the volume of a single sheet is reduced and the surface energy per volume E_s is increased. For an n -layer GaTe nanosheet, E_s could be expressed as:

$$E_s = \frac{\gamma S}{nV} = \frac{2\gamma}{nh}, \quad (5)$$

in which S , V and h represent the surface area, the volume and the thickness of a monolayer GaTe sheet, respectively. Apparently, the surface energy per volume E_s changes with the layer number n inversely, as shown in Fig. 4(b). In other words, surface energy shows increasing role as the layer number is reduced.

In brief, the interlayer interaction in bulk GaTe plays a crucial role in maintaining m-phase, while surface effect becomes prominent gradually with reducing layer thickness.

The competition between the surface effect and interlayer interaction could lead to folding, warping,²⁵ and even phase transition in 2D materials. Thermodynamically, for a GaTe sheet with a given layer number, if the total energy of the sheet in monoclinic phase, E_{m-slab} , is lower than that in hexagonal phase, E_{h-slab} , the m-phase can be stably maintained. If E_{h-slab} is lower than E_{m-slab} , phase transformation from monoclinic structure to hexagonal one might take place. Hence, the energy variation ΔE between the two phases could be used to judge the critical condition for the phase transformation. ΔE is expressed as

$$\Delta E = E_{h-slab} - E_{m-slab}. \quad (6)$$

Normally, the total energy of a GaTe sheet E_{slab} includes the energy of N pairs of Ga-Te atoms in bulk environment and the surface excess energy. The total energies of a GaTe sheet in monoclinic and hexagonal phases are expressed by the following equations, respectively.

$$E_{m-slab} = NE_{bulk}^m + \gamma_m A_{m-surf}, \quad (7a)$$

$$E_{h-slab} = NE_{bulk}^h + \gamma_h A_{h-surf}, \quad (7b)$$

in which E_{bulk}^m and E_{bulk}^h are the energy of each pair of Ga-Te atoms in m- and h-phases, respectively. Additionally, when the m-GaTe sheets are transformed into h-phase, the surface area changes, and the relationship could be depicted by

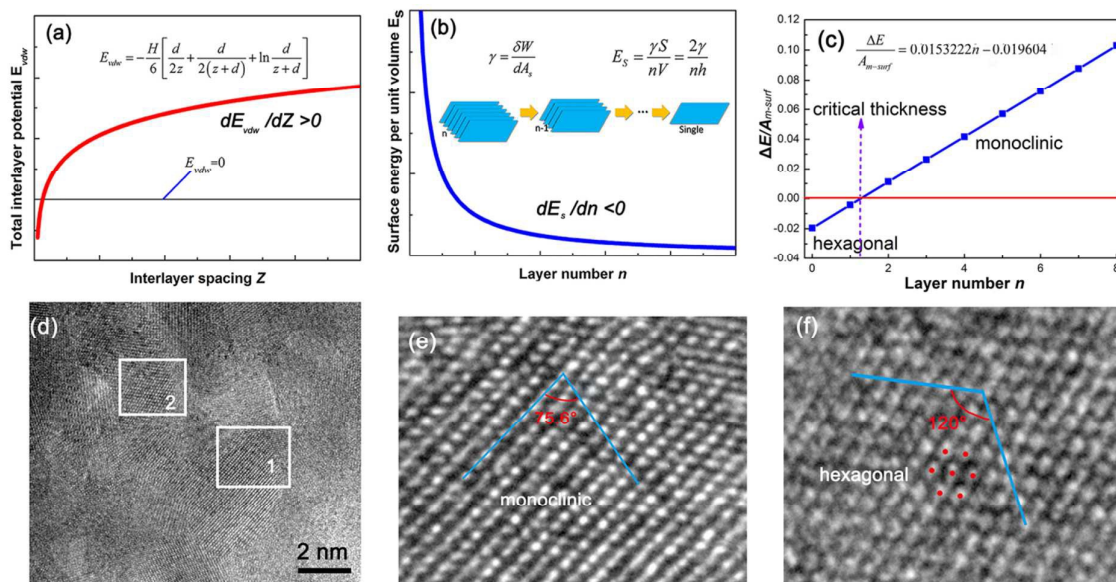


Fig. 4 (a) The relationship between total interlayer potential E_{vdw} and interlayer spacing Z . (b) Surface energy per unit area E_s vs layer number n . (c) The energy difference per surface area between the monoclinic and hexagonal GaTe. The calculated critical thickness for phase transformation is 1.27 monolayer. (d) TEM image of GaTe nanosheets, (e) and (f) The HR-TEM images of the regions 1 and 2 marked by white squares in panel (d).

$$A_{h-surf} = cA_{m-surf}. \quad (8)$$

Then, the energy variation ΔE is

$$\Delta E = N(E_{bulk}^h - E_{bulk}^m) + (c\gamma_h - \gamma_m)A_{m-surf}. \quad (9)$$

It could be rewritten as

$$\Delta E = n\rho_m \frac{A_{m-surf}}{2} (E_{bulk}^h - E_{bulk}^m) + (c\gamma_h - \gamma_m)A_{m-surf}, \quad (10)$$

where ρ_m is the surface density of atoms, i.e., the number of atoms per area, in m-phase, n is the layer number of a GaTe sheet. By using first-principle calculations, we got the bulk energies and the surface energies of GaTe in m- and h-phases, $E_{bulk}^m = -6.3588\text{eV}$, $E_{bulk}^h = -6.1127\text{eV}$, $\gamma_m = 0.02011\text{eV}/\text{\AA}^2$, $\gamma_h = 0.0005695\text{eV}/\text{\AA}^2$, respectively. Further, the energy variation ΔE can be expressed as

$$\Delta E = 0.0153222nA_{m-surf} - 0.019604A_{m-surf}. \quad (11)$$

The energy variation per surface area is

$$\frac{\Delta E}{A_{m-surf}} = 0.0153222n - 0.019604. \quad (12)$$

Fig. 4(c) displays the energy variation per surface area as a function of layer number n . The energy variation goes to zero for GaTe sheet with a thickness of 1.27 layers which is indeed the critical thickness. The difference with the experimental value may come from the long-range Coulomb repulsion between the adjacent atom layers.³⁰ When the sheet is thicker than the critical value, the energy variation is positive, that is, the total energy of the m-phase is lower than that of h-phase, and GaTe sheets exist in monoclinic lattice. As GaTe sheets are exfoliated into single-layer, the energy variation becomes

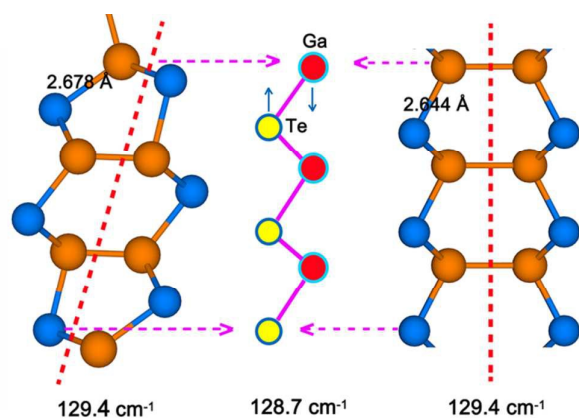


Fig. 5 The displacement vector of Raman-active mode at 128.7 cm^{-1} , and the corresponding atomic configurations in monoclinic and hexagonal structures.

negative, and the total energy of m-phase is higher than that of h-phase as a result of increased surface energy. This might lead to phase transformation from monoclinic structure [Fig. 4(e)] to hexagonal one [Fig. 4(f)] in local regions marked by the white solid squares in Fig. 4(d).

The crystal structure of m-GaTe shows strong correlation with that of h-GaTe. In monoclinic model, 6 Ga atoms and 6 Te atoms are included in each unit cell for m-GaTe in which two thirds of Ga-Ga bonds are perpendicular to the layer and one third parallel to the layer. Interestingly, all the Ga-Ga bonds have the same length of 2.43 \AA . In h-GaTe model, Ga atoms and Te atoms are arranged in a GaSe-like hexagonal structure in which the Ga-Ga bonds perpendicular to the layers are sandwiched by two Te monolayers.¹⁶ It is easy to find the similar structural characteristics of monoclinic and hexagonal lattices. First of all, both m-GaTe and h-GaTe have a layered structure which is connected by van der Waals interaction. It means that phase transformation occurs within the layers. Furthermore, some Te atoms in the same layer are arranged in six-fold symmetry in m-GaTe, the same as that in h-GaTe. Hence, it is not necessary for these Te atoms in a given layer to change their relative positions and to change the surrounding condition during the phase transformation. Results of Raman spectra consolidate the supposition that part of Te atoms are not involved in the phase transformation. Both the Raman-active peak at 129.4 cm^{-1} in 2D GaTe and that in bulk GaTe can be ascribed to the same vibration mode related to the almost unchanged Ga-Te bond length. Fig. 5 schematically presents the displacement vector due to the vibration of Ga-Te bonds and the corresponding Te atoms arranged in a hexagonal lattice. When the bulk GaTe is thinned into few-layer configuration,

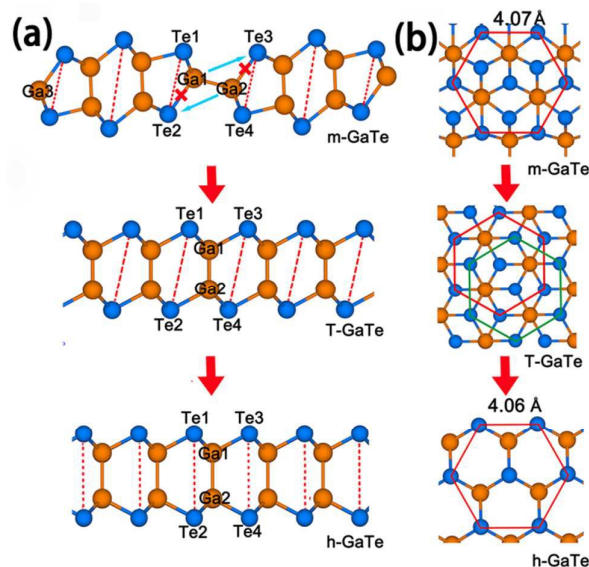


Fig. 6 Schematic illustration of the two-stage phase transformation. (a) The bond rearrangement in the phase transformation viewed from the cross-section direction. (b) The evolution of Te atom arrangements in the phase transformation viewed from the top direction.

therefore, the phase transformation can be readily found within layers as a result of weakened interlayer interaction and enhanced surface effect.

As shown in Fig. 6(a), a two-stage transformation mechanism is proposed, including m-GaTe, T-GaTe (tetragonal) and h-GaTe phases. As bulk GaTe with monoclinic structure is scaled down to few-layer flakes, the interlayer interaction is weakened and the surface effect becomes dominant. This leads to the deviation from the stable structure. The phase transition can thus happen and the process can be described as below. Firstly, Ga1-Te2 and Ga2-Te3 bonds are broken and new Ga1-Te3 and Ga2-Te2 bonds are formed. Then the Ga1-Ga2 bonds will be clockwise rotated by 90 degrees to keep parallel with other Ga-Ga bonds. As a result, m-GaTe is changed into T-GaTe. Due to the same length of the perpendicular and parallel Ga-Ga bonds, the Te monolayer shows a smooth appearance. Subsequent structure optimization leads to rearrangement of Te atoms and the unstable T-GaTe transforms into stable h-GaTe. Fig. 6(b) presents the position evolution of Te atoms from m-GaTe to h-GaTe. It is clearly observed that some Te atoms in m-GaTe are in hexagonal geometry and located in the same monolayer. When the transition from m-GaTe to T-GaTe occurs, Te atoms can be divided into two groups: one from m-GaTe and the other from the rearranged Te atoms accompanying with the rotation of Ga-Ga bonds. Consequently, the upper Te atoms are not aligned with the lower Te atoms. Then, the unstable T-GaTe changes into the stable h-GaTe. The Te atoms become aligned along [001] orientation and the two hexagonal groups develop into one. The length of the unit cell in m-GaTe, T-GaTe and h-GaTe are 11.99 nm, 12.42 nm and 12.18 nm, respectively. A structure expansion emerges during the phase transformation from m-GaTe to T-GaTe owing to the reduced interlayer interaction, where a subsequent contraction takes place due to enhanced surface effect.

As discussed above, the Raman-active mode with a frequency of 129 cm^{-1} in both m- and h- phases originates from the same Ga-Te bonds. The difference in interlayer interaction is the only factor influencing the vibration frequency. The weakened interlayer interaction in few-layer sheets reduces the effective restoring force on Ga-Te bonds and might lead to a sharp decrease of high-frequency Raman shift after the phase transformation. At the same time, there is a larger in-plane lattice constant for an overall expansion when the structure changes to be hexagonal, which could also reduce the Raman-active frequency, as shown in Fig. 3(f). The blue shift of the A_g modes can be attributed to the in-plane lattice contraction because of surface effect when the layer number is decreased. There is still no photoelectric devices based on single-layer GaTe reported,^{12-14, 31} which may be related to the indirect bandgap of h-GaTe.¹² In a word, both the experimental and theoretical results demonstrate that phase transformation from monoclinic to hexagonal might take place in few-layer GaTe sheets.

Conclusions

In summary, a spontaneous structural phase transformation from monoclinic to hexagonal was demonstrated in few-layer GaTe. Both the thermodynamic analysis and experimental characterization showed that there is a critical thickness for the phase transformation. A two-stage transformation mechanism was proposed to understand the phase transformation. An interlayer expansion occurred from m-GaTe to T-GaTe, but a contraction process took place subsequently in the phase transformation from T-GaTe to h-GaTe. Such findings reveal the crucial role of interlayer interaction on structure stability in 2D materials and provide guidance for new phase-engineered strategy in the electronic and optoelectronic applications.

Acknowledgments

This work was supported by the research fund of the State Key Laboratory of solidification processing (NWPU); The Fundamental Research Funds for the Central Universities 3102016ZY011; National Natural Science Foundation of China 51372205, 51420105005, 51271139, 51471130, 61274081. The work was also supported by State Key Laboratory for Mechanical Behaviour of Materials.

References

1. A. Splendiani, L. Sun, Y. Zhang, T. Li, J. Kim, C.-Y. Chim, G. Galli and F. Wang, *Nano Lett.*, 2010, **10**, 1271-1275.
2. S. Xu, Y. Han, X. Chen, Z. Wu, L. Wang, T. Han, W. Ye, H. Lu, G. Long and Y. Wu, *Nano Lett.*, 2015, **15**, 2645-2651.
3. J. Qiao, X. Kong, Z.-X. Hu, F. Yang and W. Ji, *Nat. Commun.*, 2014, **5**, 4475.
4. C. Lee, H. Yan, L. E. Brus, T. F. Heinz, J. Hone and S. Ryu, *ACS Nano*, 2010, **4**, 2695-2700.
5. A. Ferrari, J. Meyer, V. Scardaci, C. Casiraghi, M. Lazzeri, F. Mauri, S. Piscanec, D. Jiang, K. Novoselov and S. Roth, *Phys. Rev. Lett.*, 2006, **97**, 187401.
6. H. Li, Q. Zhang, C. C. R. Yap, B. K. Tay, T. H. T. Edwin, A. Olivier and D. Baillargeat, *Adv. Funct. Mater.* 2012, **22**, 1385-1390.
7. W. Zhao, Z. Ghorannevis, K. K. Amara, J. R. Pang, M. Toh, X. Zhang, C. Kloc, P. H. Tan and G. Eda, *Nanoscale*, 2013, **5**, 9677-9683.
8. L. Liang and V. Meunier, *Nanoscale*, 2014, **6**, 5394-5401.
9. Y. Kim, Y. I. Jhon, J. Park, J. H. Kim, S. Lee and Y. M. Jhon, *Nanoscale*, 2016.
10. F. Ma, K.-W. Xu and P. K. Chu, *Mat. Sci. Eng. R*, 2013, **74**, 173-209.
11. Y. Kondo, Q. Ru and K. Takayanagi, *Phys. Rev. Lett.*, 1999, **82**, 751.
12. F. Liu, H. Shimotani, H. Shang, T. Kanagasekaran, V. Zolyomi, N. Drummond, V. I. Fal'ko and K. Tanigaki, *ACS Nano*, 2014, **8**, 752-760.
13. Z. Wang, K. Xu, Y. Li, X. Zhan, M. Safdar, Q. Wang, F. Wang and J. He, *ACS Nano*, 2014, **8**, 4859-4865.
14. P. Hu, J. Zhang, M. Yoon, X.-F. Qiao, X. Zhang, W. Feng, P. Tan, W. Zheng, J. Liu and X. Wang, *Nano Res.*, 2014, **7**, 694-703.
15. G. Shen, D. Chen, P.-C. Chen and C. Zhou, *ACS Nano*, 2009, **3**, 1115-1120.
16. E. Finkman and A. Rizzo, *Solid State Commun.*, 1974, **15**, 1841-1845.

PAPER

Physical Chemistry Chemical Physics

17. A. Chevy, A. Kuhn and M.-S. Martin, *J. Cryst. Growth*, 1977, 38, 118-122.
18. P. M. Reshmi, A. G. Kunjomana, K. A. Chandrasekharan and M. Meena, *Int. J. Soft Comput. Eng.*, 2011, 1, 228-232.
19. A. Zubiaga, F. Plazaola, J. A. Garci, V. M. Oz-Sanjosed and C. M. Nez-Tomá, *Phys. Rev. B*, 2003, 68.
20. A. C. Ferrari and D. M. Basko, *Nat. Nanotechnol.*, 2013, 8, 235-246.
21. F. Cerdeira, E. Meneses and A. Gousskov, *Phys. Rev. B*, 1977, 16, 1648.
22. J. Irwin, B. Clayman and D. Mead, *Phys. Rev. B*, 1979, 19, 2099.
23. C. Lejon and L. Österlund, *J. Raman Spectrosc.*, 2011, 42, 2026-2035.
24. X. Yuan, L. Tang, P. Wang, Z. Chen, Y. Zou, X. Su, C. Zhang, Y. Liu, W. Wang and C. Liu, *Nano Res.*, 2015, 8, 3332-3341.
25. Y. Wang, Z. Ni, Z. Shen, H. Wang and Y. Wu, *Appl. Phys. Lett.*, 2008, 92, 043121.
26. W. Dang, H. Peng, H. Li, P. Wang and Z. Liu, *Nano Lett.*, 2010, 10, 2870-2876.
27. D. Teweldebrhan, V. Goyal and A. A. Balandin, *Nano Lett.*, 2010, 10, 1209-1218.
28. M. A. Lukowski, A. S. Daniel, F. Meng, A. Forticaux, L. Li and S. Jin, *J. Am. Chem. Soc.*, 2013, 135, 10274-10277.
29. E. Yoo, J. Kim, E. Hosono, H.-s. Zhou, T. Kudo and I. Honma, *Nano Lett.*, 2008, 8, 2277-2282.
30. T. Wieting and J. Verble, *Phys. Rev. B*, 1972, 5, 1473.
31. Z. Wang, M. Safdar, M. Mirza, K. Xu, Q. Wang, Y. Huang, F. Wang, X. Zhan and J. He, *Nanoscale*, 2015, 7, 7252-7258.